Evaluation of L-band GPS signal attenuation to multiple vegetations using ground-based measurements

Evaluation of L-band GPS signal attenuation to multiple vegetations using ground-based measurements

Yan Jia[a], Shuanggen Jin [b,c*], Zhiyu Xiao[a], Qingyun Yan[b] Wenmei Li[a] and Patrizia Savi[d]

[a] Department of Surveying and Geoinformatics, Nanjing University of Posts and Telecommunications, Nanjing, China, 210046;[b] School of Surveying and Land Information Engineering, Henan Polytechnic University, Jiaozuo, China, 454000; [c] Shanghai Astronomical Observatory, Chinese Academy of Sciences, Shanghai, China, 200030; [d] Politecnico di Torino, Corso Duca degli Abruzzi 24, Torino, Italy, 10129.

***** Correspondence**,** E-mail: sgjin@nuist.edu.cn

Yan Jia received a double M.S. degree in telecommunications engineering and computer application technology from Politecnico di Torino, Turin, Italy, and Henan Polytechnic University, in 2013. She received her Ph.D. degree in Electronics Engineering from Politecnico di Torino in 2017. Now she is an associate professor working at the Nanjing University of Posts and Telecommunications. In 2013, she was in the Department of Electronics and Telecommunications, Politecnico di Torino, Torino, Italy, where she performed research on the GNSS system construction and GNSS antenna analysis. In 2014, she worked on the SMAT project, mainly focusing on the retrieval of soil moisture and vegetation biomass content by GNSS-R. Her research interests include microwave remote sensing, soil moisture retrieval, Global Navigation Satellite System Reflectometry (GNSS-R) applications to land remote sensing, and antenna design.

Shuanggen Jin was born in Anhui, China, in September 1974. He received a B.Sc. degree in Geodesy from Wuhan University, Wuhan, China in 1999 and a Ph.D. degree in Geodesy from the University of Chinese Academy of Sciences, Beijing, China in 2003. He is Vice-President and Professor at Henan Polytechnic University, China and also Professor at Shanghai Astronomical Observatory, CAS, China. His main research areas include satellite navigation, space geodesy, remote sensing, and space/planetary exploration. He has published over 500 papers in peer-reviewed journals and proceedings, 20 patents/software copyrights and 12 books/monographs with more than 11000 citations and H-index>54. He has received 100-Talent Program of CAS, World Class Professor of Ministry of Education and Cultures, Indonesia,

Fellow of IAG, Fellow of IUGG, Fellow of African Academy of Sciences, Fellow of Electromagnetics Academy, Member of Russian Academy of Natural Sciences, Member of European Academy of Sciences and Member of Academia Europaea.

Evaluation of L-band GPS signal attenuation to multiple vegetations using ground-based measurements

Abstract: Global Navigation Satellite System Reflectometry (GNSS-R) is a remote sensing technique that can be regarded as a bistatic radar system. GNSS-R uses GNSS signals as signal sources and obtains the Earth's surface environmental parameters, such as soil moisture (SM), by receiving the L-band microwave signal reflected from the Earth's surface. However, surface vegetation could be one of the main factors influencing the accuracy of GNSS-R land applications since plants, including branches and leaves, attenuate GNSS signals. Additionally, the evaluation of signal attenuation caused by the plant canopy is quite difficult. In this paper, we study the attenuations of received L1- and L2-band GPS signals to the vegetation leaf area index (LAI) for different types of plants. The relationship between the attenuation of the GPS signal-to-noise ratio (SNR) (both above and below the canopy) and the LAI is established through field experiments. The results show that the mean SNR received in the L2 band is lower than that in the L1 band for each satellite but with a larger standard deviation (SD). The sensitivities of L1- and L2-band signals to the LAI are revealed, revealing greater sensitivity and a relatively good Pearson correlation coefficient (R) for lower elevation angles and vegetation biomass. In addition, the sensitivity and R of L2-band signals to the LAI are lower than those of L1-band signals. This study is significantly valuable for improving the quantitative representation of error estimates for GNSS-R SM retrieval. The established model can be employed in GNSS land applications and aid in solving signal surface-scattering problems in which accurate signal estimates are important.

Keywords: Global Navigation Satellite System-Reflectometry (GNSS-R), Soil Moisture Retrieval, Signal-to-Noise Ratio (SNR), Vegetation, Leaf Area Index (LAI).

1. Introduction

Global Navigation Satellite System-Reflectometry (GNSS-R) is an Earth observation technology that uses GNSS signals reflected from the Earth’s surface to remotely sense the ocean, land, cryosphere, and other surface parameters (Jin et al. 2011). Using the GNSS constellation as a multisource L-band microwave transmission source, the electromagnetic GNSS waves reflected

from target objects can be obtained by using ground, space-based, and even space-borne GNSS receivers (Nasser et al. 2013). The GNSS signals are transmitted by many different satellite systems, including GPS, the Beidou Navigation Satellite System (BDS), Galileo, and GLONASS (Lu et al. 2020; Ban et al. 2017; Li et al. 2019). Among them, GPS was the first system to be developed (originating in the 1960s) and has been widely used to acquire GNSS-R measurements (Lowe et al. 2002). GPS satellites transmit signals at two frequencies, namely, in the L1 (1575.42 MHz) and L2 (1227.60 MHz) bands. Each signal is composed of a carrier, ranging code, and navigation message (Lowe et al. 2002).

Having become an extensively popular research topic in recent years, GNSS-R technology has thus far been successfully applied to measure sea wind (Foti et al. 2015; Clarizia et al.2014; Ruf et al. 2018), sea ice thickness (Yan et al. 2019; Rodriguez-Alvarez et al. 2019; Yan et al. 2020; Li et al. 2017), snow depth (Jin et al. 2017), and soil moisture (SM) (Chew et al. 2018; Clarizia et al. 2019; Eroglu et al. 2019; Senyurek et al. 2020; Jia et al. 2021; Yan et al. 2020; Chew et al. 2020; Calabia et al. 2020). The state of the target is retrieved by analyzing the changes in parameters such as the signal intensity, frequency, phase, and polarization direction between the reflected signal and the direct signal. The ideal case is there are no obstacles between the satellite transmitter and receivers, but the vegetation could be the most common factor affecting the surface parameters retrieval accuracy.

Vegetation constitutes a major terrestrial ecosystem, and the vegetation canopy structure (number and distribution of leaves) is fundamental to the global exchanges of both energy and carbon and to the water cycle. The leaf area index (LAI), generally defined as one-half of the total green leaf area per unit horizontal ground surface area, is one of the most effective indicators for

quantitatively describing the vegetation canopy structure (Fang et al. 2014; GCOS 2011; Watson 1947; Larson et al. 2010). Accordingly, this indicator forms the basis for studying many key ecological processes such as leaf photosynthesis, respiration, canopy interception of precipitation, and water transpiration (Aria et al. 2007). In particular, in process-based ecosystem models and quantitative remote sensing analyses, the ability to directly describe the seasonal dynamics of the LAI determines the reliability and accuracy of vegetation–air interface materials and energy exchanges (Asner et al. 2003; Waring and Running 2007). Therefore, the LAI is one of the main parameters connecting ecological processes on different scales, and rapid and accurate LAI acquisitions can provide basic data for research on vegetation restoration, global climate change, and forest management (Gholz 1982; Law et al. 2001).

To date, two methods have been widely used to analyze the vegetation canopy: foliage harvesting and scanning (Chen et al. 2018). Between these two techniques, foliage harvesting has been the method of choice for analyzing the vegetation canopy, and the data obtained by this method are considered to be the most accurate. In contrast, scanning is more efficient. Although these two methods were widely used in the early years, they still suffer from some drawbacks in measuring the vegetation canopy; for example, foliage harvesting damages plants, and it is cumbersome to scan each leaf. Consequently, satellite remote sensing technology has also been employed to investigate the vegetation canopy and measure the LAI. However, this approach also encounters some difficulties when distinguishing small patches of vegetation between satellite images, which results in measurement errors.

Due to the limitations of these methods, an instrument called the Plant Canopy Analyzer (PCA) was developed in the United States to measure the projected light intensity at five different

zenith angles above and below the tree canopy using a fisheye optical sensor. Then, a radiative transfer model of the vegetation canopy is used to calculate the canopy structural parameters, such as the effective LAI. Although it is widely believed that the authentic LAI values obtained from direct measurements are more accurate than optically determined LAI values, many experiments have validated the performance and therefore the feasibility of this instrument in measuring the parameters of plant canopies. For instance, the results obtained with the LAI-2000/2200 PCA closely approximated those derived from the foliage harvesting method (Asner et al. 2003; Behera et al. 2015). Accordingly, PCA sensors have been widely used to analyze plant canopies in agriculture and forestry.

To date, most experiments for GNSS-R land applications, such as SM retrieval, have been performed considering an ideal situation of bareness and smoothness. This assumption means no vegetation on the ground except considering the roughness effects. Otherwise, the computation of SM will be very complex. Moreover, the effects of vegetation are difficult to estimate since the plants, including branches and leaves, attenuate the GPS signal. In previous studies, some theoretical simulations were conducted to assess the relevant features and the potential for eliminating the vegetation effects in the GNSS-R working L band (Wu and Jin 2014; Ferrazzoli et al. 2000; Ferrazzoli et al. 2011). A Bi-Mimics bistatic scattering model (Wu and Jin 2014) was proposed to simulate the scattering characteristics of crops in the L band. The scattering response properties to vegetation canopies were studied, and it was shown that the received power was sensitive to forest biomass without the typical saturation of radar backscattering measurements.

Because of the complexity of vegetation scattering models, no model can simulate various vegetation types well. Even the same model can hardly simulate microwave scattering at different

growth stages well (Camps et al. 2018; Camps et al. 2016; Carreno-Luengo et al. 2019; Rodríguez-Fernández et al. 2019). Estimating and correcting the vegetation effects for received signals is difficult. Little work has been conducted to estimate the degree of the attenuated signals caused by different vegetation canopies in GNSS-R experiments. Hence, this study proposes to explore the influence of multiple vegetation covers on received GPS signals, parameterized as a function of the LAI, and it builds signal attenuation models over different plant types.

The main works of this paper are summarized as follows.

(1)An extensive ground-based experiment was specially designed for investigating vegetation characteristics and GPS L-band signals.

(2)A comprehensive qualitative analysis was performed considering both the L1 and L2 bands signals and different vegetation types.

(3)The provided qualitative relationship provides a theoretical reference for investigating other GNSS-R or scattering-related scenarios.

The article is organized as follows. Section 2 describes the theory and methods. Section 3 presents the experimental setup and data collection. The results and analysis are shown in Section 4. Finally, Section 5 summarizes the main conclusions.

2. Theory and Methods

2.1. GNSS-R SM Retrieval Configuration

Studies have shown that L-band signals have strong penetration and low attenuation and are very sensitive to SM information; hence, the applications of GNSS-R on the land surface are focused mostly on SM retrievals (Njoku and Entekhabi 1996). Different SM retrieval schemes were proposed with different polarization configurations are shown in Figure 1 (Egido et al. 2012;

Masters et al. 2004; Zavorotny et al. 2016; Jia et al. 2016; Larson et al. 2010; Alonso-Arroyo et al. 2014; Alonso-Arroyo et al. 2014; Camps et al. 2020; Mehrez et al. 2018; Mehrez et al. 2017; Alonso-Arroyo et al. 2016; Rodriguez-Alvarez et al. 2012). The reflected signal was collected from a different orientation of the surface to retrieve the SM information.

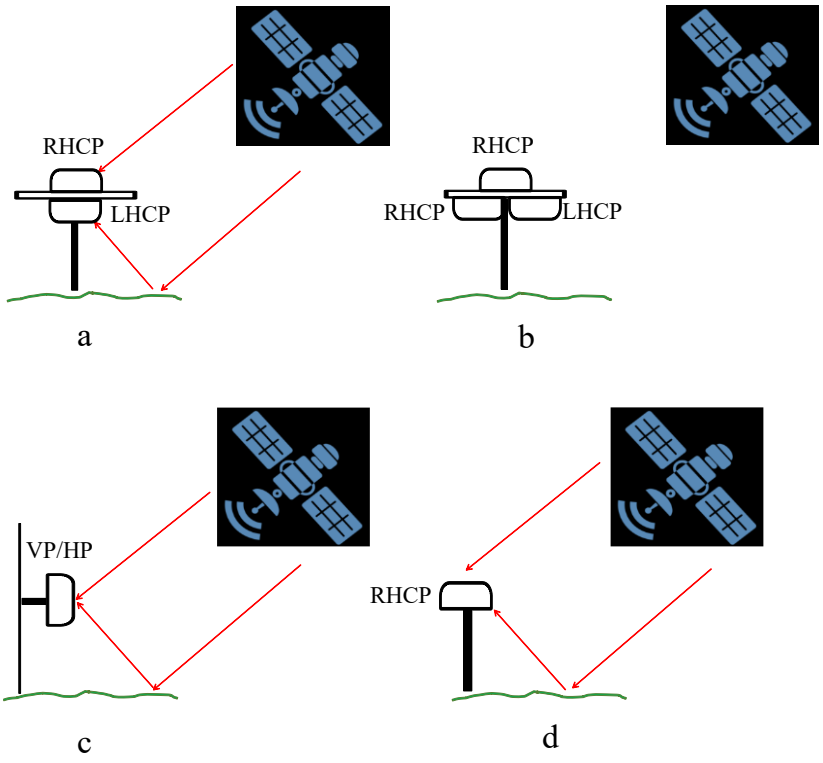

Figure 1. Receiving strategies (right-hand circular polarized (RHCP), left-hand circular polarized (LHCP), and vertically and horizontally polarized (VP and HP, respectively)) for GNSS-R SM retrievals.

It is worth noting that all receiving configurations feature signals reflected from the surface, and a radar signal emitted at a single frequency is strongly affected by the surface type (bare or vegetated land). Hence, the receiving reflectivity $\Gamma_{lr}(\theta)$ can be computed by correcting the reflection coefficient $R_{lr}(\theta)$ for the effects of vegetation and surface roughness.

The received reflectivity $\Gamma_{lr}(\theta)$ can be modeled by the following equation (Jia et al. 2016):

$$\frac{SNR_{peak}^{reflect}}{SNR_{peak}^{direct}} = \frac{r_3^2}{(r_1 + r_2)^2} |\Gamma_{lr}|^2 \ C \tag{1}$$

where C is a calibration parameter summarizing the uncertainties in receiver gain G and noise power PN. SNR_{peak} is the processed peak signal-to-noise ratio (SNR) between the direct and reflected signals and is strongly impacted by the reflecting surface, e.g., the vegetation canopy, which is investigated in this study.

2.2. Leaf Area Index (LAI) Measurement

The optical determination of indirect LAI measurements is referred to as the effective LAI (LAI_{eff}) (Vincent et al. 2017) because branches and stems intercept light (Behera et al. 2015) and limit the signal transmitted to optical devices (Chen and Black 1992; Welles and Cohen 1996). Therefore, the LAI obtained with the PCA instrument in this study is, in fact, LAI_{eff}, which can be calculated from the canopy porosity (Vincent et al. 2017; Chen and Black 1992):

$$LAI_{eff} = 2 \int_0^{\frac{\pi}{2}} In[1/p(\theta)] cos\theta sin\theta d\theta \tag{2}$$

where $p(\theta)$ represents the porosity when the zenith angle θ is zero.

PCA instruments such as the LAI-2200/2200C have become quite popular and thus have been widely adopted for acquiring LAI measurements (Vincent et al. 2017). A fisheye optical sensor (vertical field of view: 148°; horizontal field of view: 360°) is used to measure the projected light intensity at five different zenith angles (7°, 23°, 38°, 53°, and 68°) above and below the plant canopy, as shown in Figure 2. Then, a software of radiative transfer model for the vegetation

canopy is applied to calculate the LAI or other vegetation indices (Zhang et al. 2005). Hence, a normal LAI acquisition should have at least ten sampled values, namely, five values above and five values below the canopy. Usually, the five sampled values above the canopy are regarded as the "A" values, and the five sampled values below the canopy are regarded as the "B" values. The LAI can be calculated according to the sampled values of the upper and lower canopy corresponding to the five different zenith angles.

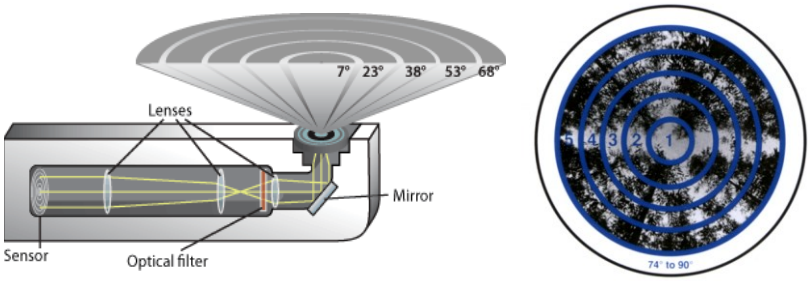

Figure 2. Schematic diagram of measuring five zenith angles.

2.3. Designation of Measuring Signal Attenuation and Plant Canopy Parameters

As mentioned above, due to the effects of vegetation on the surface, the applicability of the theoretical vegetation model is considerably limited. In addition, the intrinsic relationships between the vegetation canopy and signal attenuation are not well understood. Hence, we proposed exploring the relationship between the attenuated signals and LAIs through field experiments. With the designed experiments, the sensitivity of the GPS signals to the vegetation canopy can be revealed. Furthermore, the present fitting model can quantify the effects of different plant types on GPS signals. Figure 3 shows the designed scheme for transmission links between the transmitter and receiver based on the GNSS system.

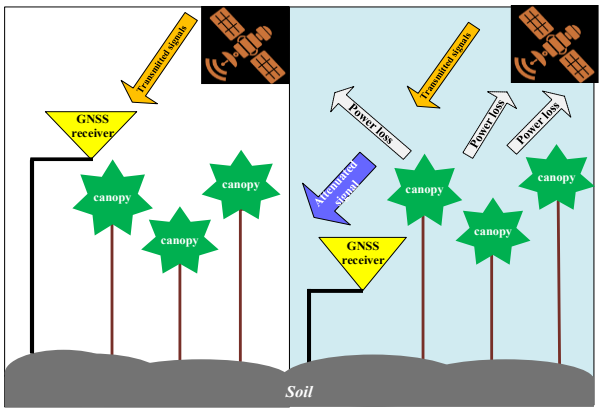

Figure 3. Schematic diagram of the designed GNSS measurement setup.

The GNSS-R receiver was designed to receive the signals from both above and below the plant canopy. Thus, the signal attenuation can be regarded as the difference between the SNRs of these two signals. The following equations represent the transmission paths of the two received signals (above and below the canopy) under the influence of the vegetation canopy:

$$p_{GNSS}^{above} = p_{Rh}^{gps} \tag{3}$$

$$p_{GNSS}^{below} = p_{Rh}^{gps} - p_{veg}^{loss}(lai) \tag{4}$$

$$p_{GNSS}^{above} - p_{GNSS}^{below} = p_{veg}^{loss}(lai) \tag{5}$$

where p_{GNSS}^{above} stands for the received signal power without the effect of vegetation and p_{GNSS}^{below} represents the signal power after penetrating through the vegetation canopy. The subscript Rh symbolizes the right-hand polarization transmitted by GPS satellites. In this way, the relationship between signal attenuation and the vegetation LAI can be established, as shown in (5). Figure 4 shows a flowchart of the process designed for the proposed measurement and modeling of the LAI and signal attenuation. Measurements were carried out to obtain the GPS signals and LAI (above

and below the canopy) over different plants. Then, the sampled values were used to obtain different fitting models revealing the sensitivity of the LAI to signal attenuation in the L1 and L2 bands. The details regarding the equipment setup and data collection procedure are presented in the following section.

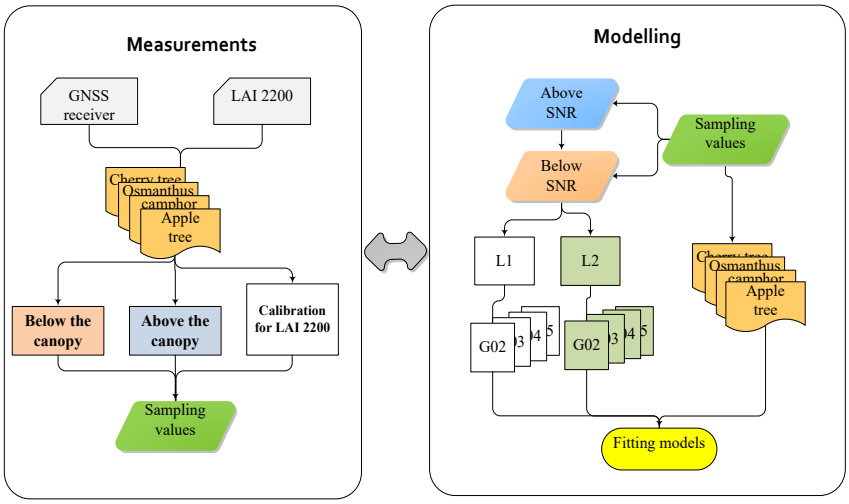

Figure 4. Flowchart for measuring and modeling GPS signal attenuation and the LAI.

3. Measurement Setup and Data Collection

3.1. GNSS Receiver

A dual antenna positioning GNSS receiver M600 developed by ComNav Technology Ltd. was employed in this study (Chen and Black 1992). The receiver is based on ComNav's high-precision multimode multiband proprietary receiver, can track 14 satellites for each satellite system with multiple frequencies, and has a carrier phase positioning accuracy of 0.5 mm. It features a flexible design and built-in wireless radio module for flow operations. The GNSS receiver provided two ports for receiving signals simultaneously to avoid synchronization issues. Two high-gain RHCP antennas were used to receive satellite-transmitted signals above and below the canopy. The

sampling data was transferred to a PC for data storage via two output ports.

An important parameter with respect to the GPS antenna is the half-power beam width (HPBW), which is the angular separation in which the magnitude of the radiation pattern decreases by 50% (or -3 dB) from the peak of the main beam. The measured power in this study is the power received by the antenna after being transmitted through the vegetation layer of the trees. A value lower than a certain value cannot be collected by the antenna, which is outside the antenna's footprint. Hence, the HPBW requirement was created to define the antenna's footprint and to ensure that the power can be observed contemporaneously. Thus, the received power should be in the range of the antenna's footprint, which is strictly related to the HPBW.

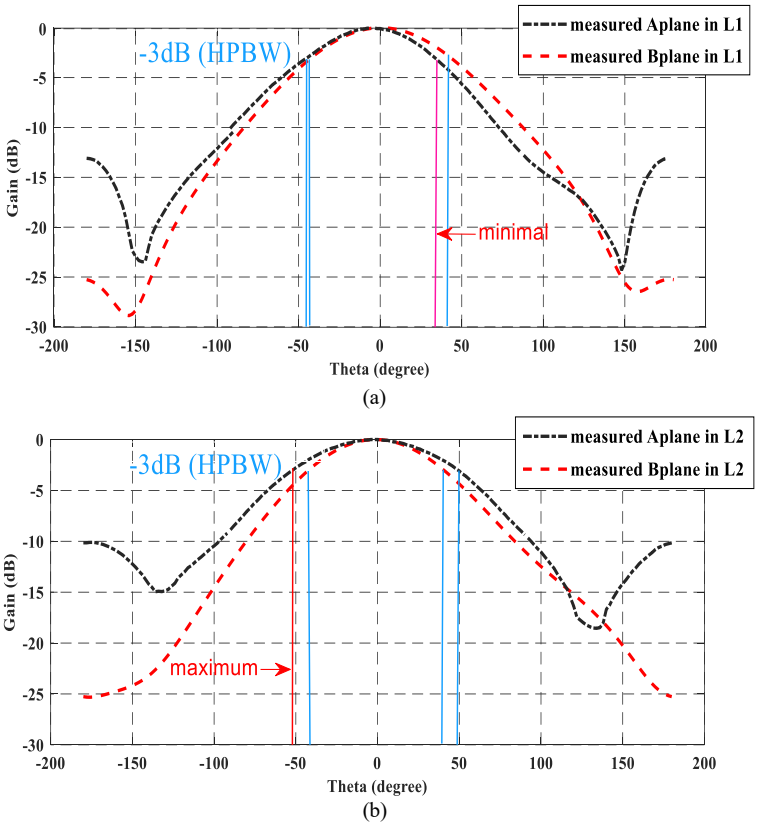

Figure 5. The measured radiation pattern for L1(a) and L2 (b) bands with two orthogonal planes.

Figure 5 depicts the radiation patterns of the employed antenna measured in an anechoic chamber. The HPBW ranges from 70° to 106°. HPBW = 70° means that the requirement of the minimum elevation angle of the satellite is 55°. In this study, with different sizes of tree canopies, we adjust the antenna height to ensure that the received signal satisfies the geometrical requirement. The received signals can penetrate through the tree canopy and fall into the antenna's footprint, which is defined by the HPBW.

3.2. LAI-2200C PCA

LAI-2000 and LAI-2200/2200C PCAs (Welles and Cohen 1996) have been widely used for indirect LAI measurements. With the LAI-2000 or LAI-2200/2200C PCA, the readings of light information from five different zenith angles can be obtained at a given time, with the optical sensor positioned either above or below the canopy (Welles and Cohen 1996). The adopted advanced LAI-2200C PCA (Figure 6) is based on the mature LAI-2000/2200 technology platform with a built-in GPS module integrated with GPS information. Moreover, it provided the scattering calibration procedure, which can make the results more accurate. Hence, the LAI-2200C plant canopy analyzer is suitable for any canopy measurement under any sky conditions and has been used widely in LAI estimation retrieval and validation.

Figure 6. LAI-2200C PCA for LAI measurements.

3.3. Scattering Correction and Data Collection

The campaign was carried out at the campus of Nanjing University of Posts and Telecommunications from May 13-15, 2021, and the campus is located in the coastal part of China (32°7'16 N, 118°56'7 E). This site is a large area covered by many kinds of plants. Eight types of trees, including camphor, osmanthus, purple-leaf plum, oak, cherry, begonia, magnolia, and apple trees, were selected for LAI measurements. These trees have different profiles, which can be arranged in order of leaf size from small to large, which corresponds to the photo from left to right, as shown in Figure 7. One reason for choosing these types of trees is that the height of the trees is moderate, as is the luxuriant degree of the canopy. Another reason is that the canopy is considered normal and is easy to identify. Hence, it is convenient for the experiment and beneficial to the accuracy of the experimental results.

Figure 7. Observed tree examples for LAIs and receiver experiments.

As mentioned above, the ground LAI_{eff} was measured with an LAI-2200C PCA (Li-Cor, Lincoln, Nebraska, USA), which is an indirect non-contact instrument used to measure the gap fraction of the diffuse radiation transmission observed through the canopy (Chen and Cihlar 1996; ComNav Technology Ltd. 2022), as shown in Figure 8. The measurements were performed near sunrise or sunset to obtain nearly uniform sky illumination. When the weather condition is clean and transparent with a blue sky or there are thin clouds and sun, sunlight will increase the scattering error, so scattering correction is required. Here, all the plant canopy measurements were obtained with scatter correction to remove the effect of weather on different types of trees.

Three types of data are required for scattering correction: blue light band characteristics (generally used the Default value), *K* value, and GPS data. Assume that the measurement sequence is "ABBB" when measuring without scattering correction, and "4A" is required to replace "A" when measuring with scattering correction, so the measuring sequence is "AAAABBBB". The first "A" value: white scattering cap, direct sunlight; The second "A" value: white scattering cap, shading (self-projection or hand); The third "A" value: open the field of vision as far as possible, with no covering cap (or 270 ° covering cap), and shade. The fourth "A" value: normal cover cap, and normal measurement direction (that is, the measurement method is the same as that of the "B" value). After the measurement is completed, import the data to the corresponding software to compute the scattering correction parameter *K*.

For each LAI measurement unit, four above-canopy "A" and several below-canopy "B" LAI-2200C operations were performed for scattering calibrations and to obtain one local LAI value. The number of measured B values needs to be determined by canopy height as shown in the following equation (Vincent et al. 2017; Chen and Black 1992):

$$A = f\pi H^2 \quad (6)$$

where A represents the sampling area, f is the viewing angle range (0.75, 0.5, 0.25, and 0.125 represent 270 °, 180 °, 90 ° and 45 ° covering caps respectively), and H is the canopy height. It is determined by the change in blade density at the measuring point. The following is the specific method to determine the number of B values in this experiment.

(1) Six B values are used to determine an LAI_{eff} to ensure that it contains the thinnest and densest part of the crown;

(2) Calculate SEL/LAI_{eff} (SEL is the standard error of LAI_{eff});

(3) Use Table 1 to determine the number of B values.

Table 1 The determination of the number of B values

SEL/LAI_{eff}	#B Readings	SEL/LAI_{eff}	#B Readings
0.01	2	0.06	11
0.02	3	0.07	13
0.03	5	0.08	16
0.04	6	0.09	19
0.05	8	0.1	23

The GNSS receiver is set up simultaneously to receive the GPS signals at the same survey point. The receiver was designed to connect two antennas to receive signals from above the canopy and below the canopy. The above-canopy signal is received by one RHCP antenna placed in the open area one meter away from the tree trunk at a low position to avoid different heights being received and to keep the equipment stable and the measurements accurate. Another RHCP antenna was located just below the tree, as shown in Figure 8.

Figure 8. LAI measurements were obtained with an LAI-2200C PCA (left) and GNSS signal receiver (right).

Additionally, three different canopy sizes are considered for each tree type. For each canopy size, sampling operations were repeated three times (three LAI values) and averaged for obtaining one more accurate LAI value representing one tree canopy size. Hence, from eight field campaigns, 72 sampling units of measurement data were collected. The distribution of the measurements is shown on a China street colour maps to illustrate the experimental area and locations (Figure 9).

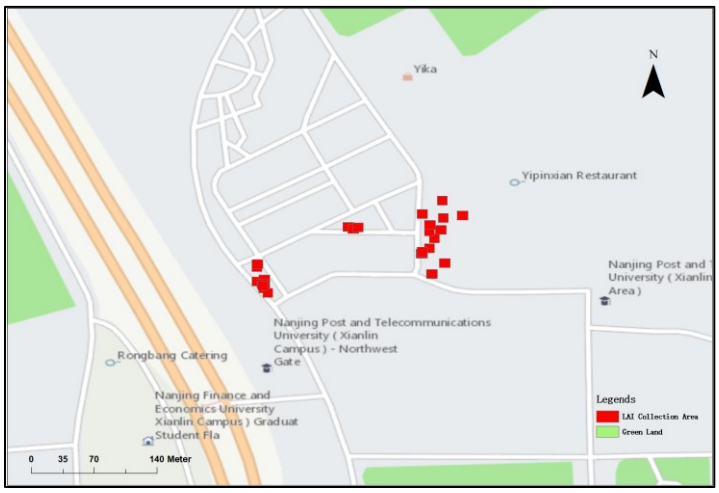

Figure 9. LAI and GNSS signal receiver measurement locations on China street color maps.

4. Results and Analyses

4.1. GPS L1 and L2-Band Signal Tracking

The GNSS receiver was employed to track GPS signals above and below the canopy. The positions of the tracking satellites are shown in Figure 10, and the received SNRs from these two positions are plotted in Figure 11. Because of the large number of measurements during the campaign, the results of only one sampling unit are illustrated as an example for each tree.

In Figure 10, the satellite positions during data collection are plotted with sky plots. Sky plots show the positions of satellites in terms of elevation and azimuth. The elevation is presented by the concentric rings nested within one another. The outside ring is 0°, and the middle of the plot is at a 90° elevation. The azimuth is the direction angle measured clockwise in relation to north (0°). Each series of points represents a certain PRN. The signal power and the attenuation of the GNSS are dependent on the vegetation penetration path as well as the antenna pattern (HPBW) and elevation angles. Thus, the results are presented considering satellites with elevation angles of 55°-90° to ensure that the received power penetrates through the plant canopy and falls within the antenna's footprint.

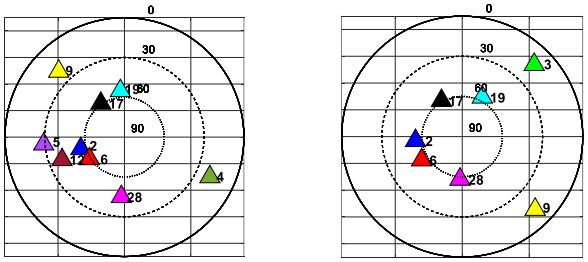

(a) **(b)**

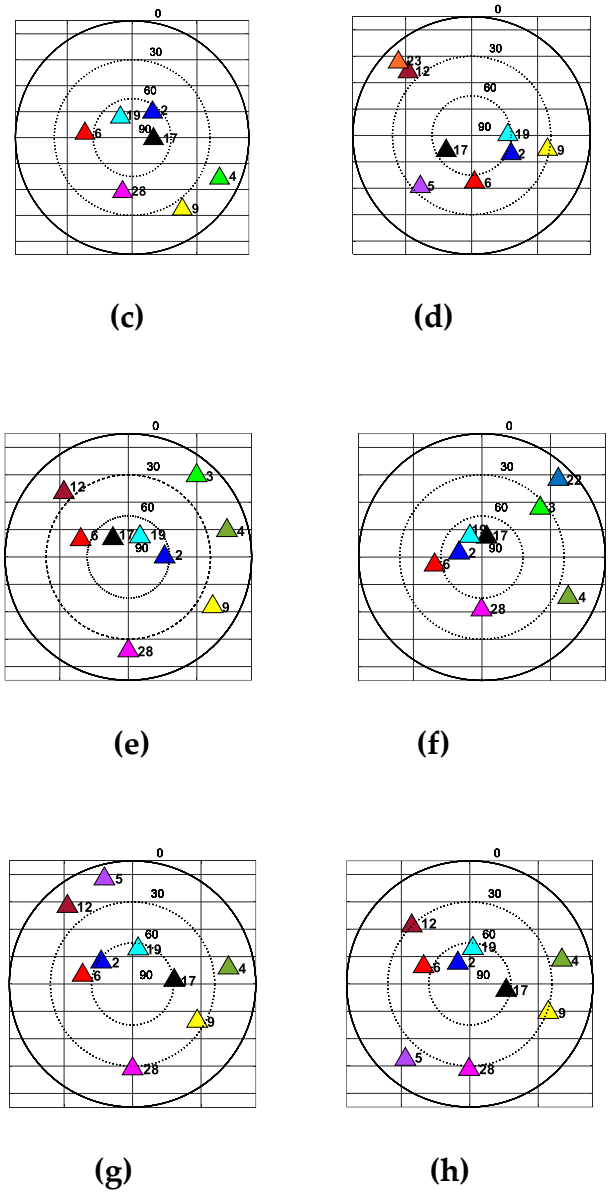

Figure 10. Eight Sky-plot examples for GPS satellite L1 and L2 bands during the experiments: (a) osmanthus tree, (b) camphor tree, (c) purple-leaf plum tree, (d) oak tree, (e) begonia tree, (f) magnolia tree, (g) apple tree, and (h) cherry tree.

The signals both below and above the canopy were acquired at the same time by a dual polarization receiver. Thus, the data discrepancy and deviations can be mostly removed due to the

difference in time, samples, or locations, and the absolute attenuation caused by the plant canopy can be extracted. For illustration purposes, examples of received above- and below-canopy SNR signal levels are presented in Figure 11, corresponding to the eight observed tree types. In Figure 11, the L1 band SNR below the canopy (blue), the L1 band SNR above the canopy (red), the L2 band SNR below the canopy (green), and the L2 band SNR above the canopy (yellow) from the GNSS receiver are presented. The SNR received below the canopy is lower than the signals received above the canopy in both the L1 and L2 bands, which preliminarily shows that the plant canopy strongly affects the signal strength and hence could be one of the main factors influencing GNSS-R applications.

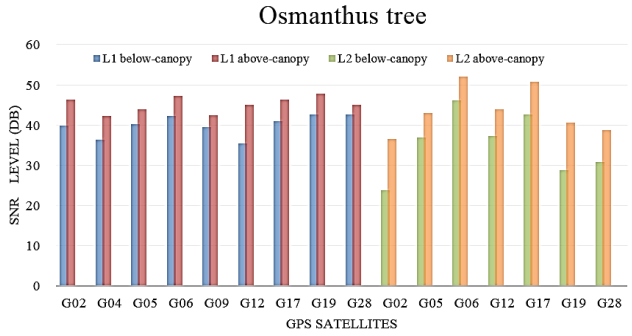

(a)

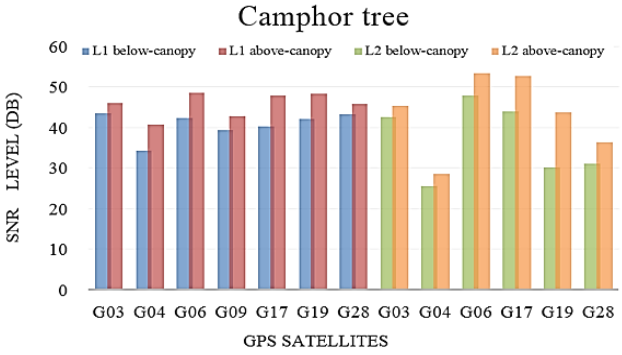

(b)

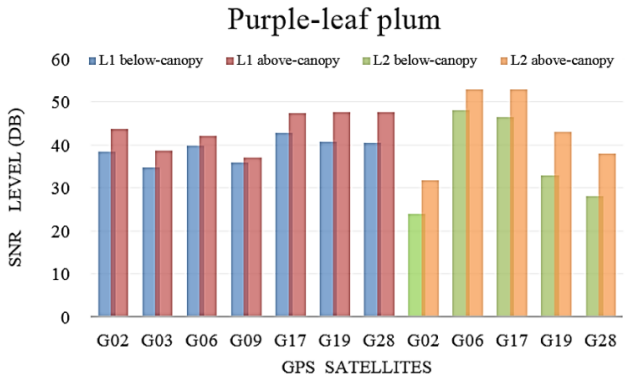
Purple-leaf plum
L1 below-canopy
L1 above-canopy
L2 below-canopy
L2 above-canopy
SNR LEVEL (DB)
60
50
40
30
20
10
0
G02 G03 G06 G09 G17 G19 G28 G02 G06 G17 G19 G28
GPS SATELLITES

(c)

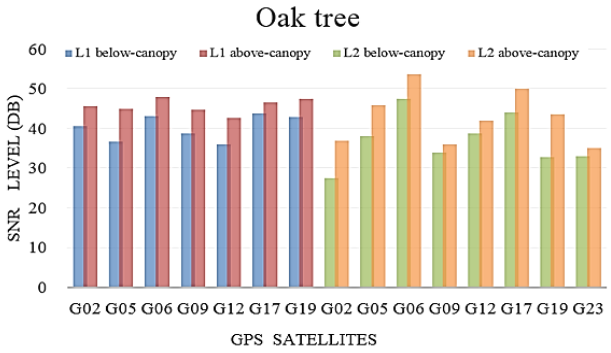
Oak tree
L1 below-canopy
L1 above-canopy
L2 below-canopy
L2 above-canopy
SNR LEVEL (DB)
60
50
40
30
20
10
0
G02 G05 G06 G09 G12 G17 G19 G02 G05 G06 G09 G12 G17 G19 G23
GPS SATELLITES

(d)

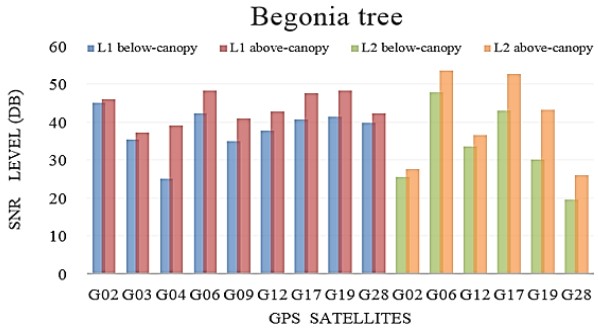
Begonia tree
L1 below-canopy
L1 above-canopy
L2 below-canopy
L2 above-canopy
SNR LEVEL (DB)
60
50
40
30
20
10
0
G02 G03 G04 G06 G09 G12 G17 G19 G28 G02 G06 G12 G17 G19 G28
GPS SATELLITES

(e)

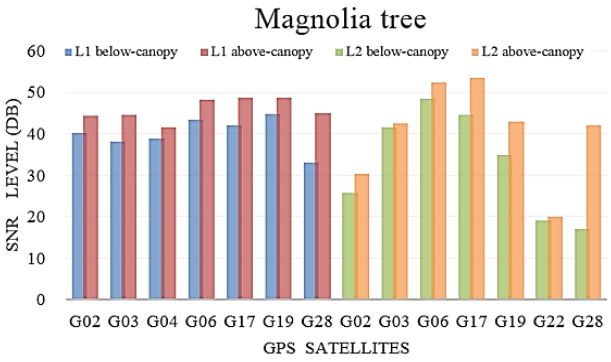
Magnolia tree
L1 below-canopy
L1 above-canopy
L2 below-canopy
L2 above-canopy
SNR LEVEL (DB)
60
50
40
30
20
10
0
G02 G03 G04 G06 G17 G19 G28 G02 G03 G06 G17 G19 G22 G28
GPS SATELLITES

(f)

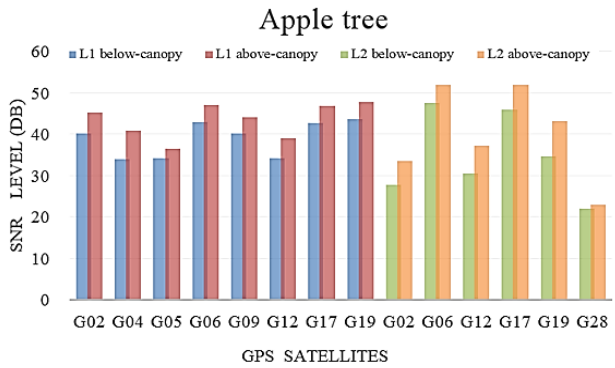
Apple tree
L1 below-canopy
L1 above-canopy
L2 below-canopy
L2 above-canopy
SNR LEVEL (DB)
60
50
40
30
20
10
0
G02 G04 G05 G06 G09 G12 G17 G19 G02 G06 G12 G17 G19 G28
GPS SATELLITES

(g)

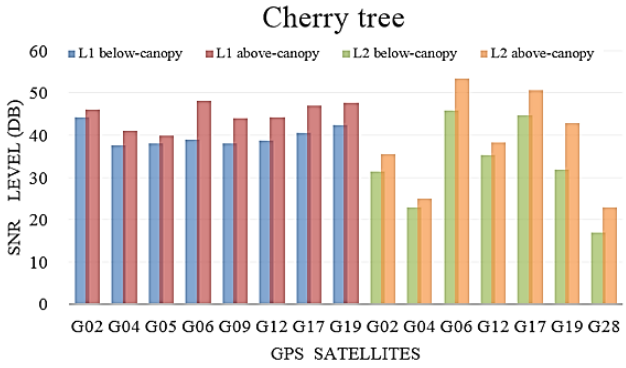
Cherry tree
L1 below-canopy
L1 above-canopy
L2 below-canopy
L2 above-canopy
SNR LEVEL (DB)
60
50
40
30
20
10
0
G02 G04 G05 G06 G09 G12 G17 G19 G02 G04 G06 G12 G17 G19 G28
GPS SATELLITES

(h)

Figure 11. Eight SNR examples for the GPS L1 and L2 bands: (a) osmanthus tree, (b) camphor tree, (c) purple-leaf plum tree, (d) oak tree, (e) begonia tree, (f) magnolia tree, (g) apple tree, and (h) cherry tree.

4.2. Above- and Below-Canopy GPS L1- and L2-Band Signals

After preprocessing and collecting the experimental data described above, the scatter plots of all received SNR levels are plotted in Figure 12 for each tree type to ensure robust fitting (Li-Cor 1992; Chen et al. 1997; Welles and Norman 1991; Li et al. 2017; Holland and Welsch 1997). The results of the sampling units, including the below- and above-canopy signal comparison diagram in the L1 and L2 bands, are considered. As shown in Figure 11, the SNR below the canopy is lower than the SNR received above the canopy, which is observed from both the L1 and L2 bands. Further statistical results are presented with a boxplot (Figure 13).

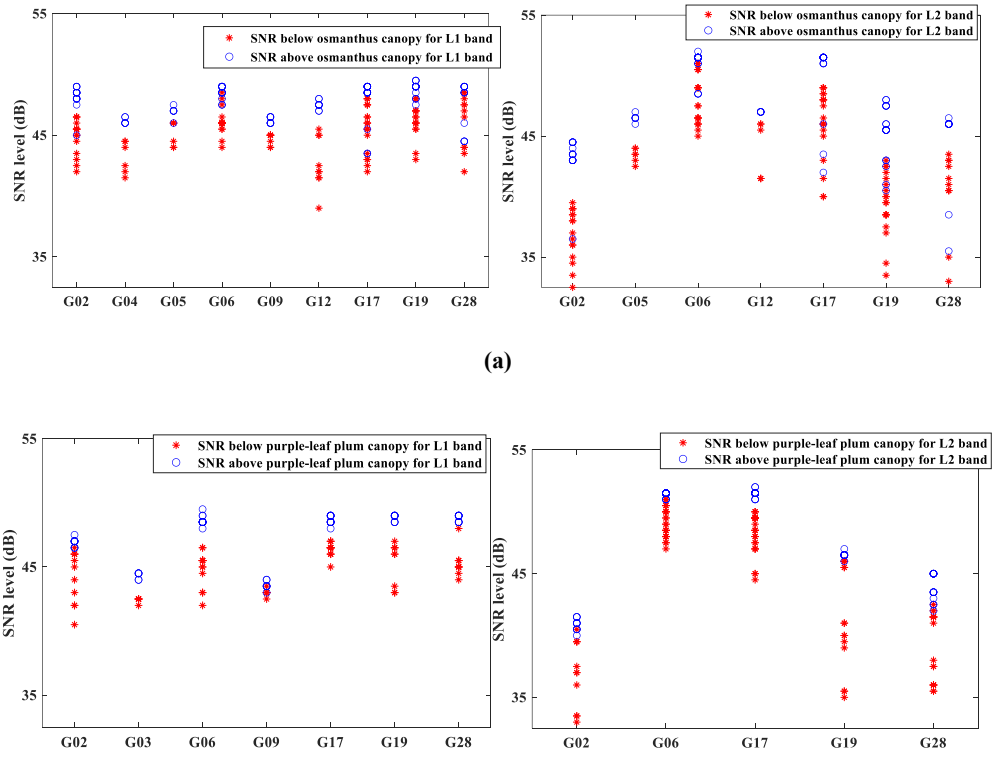

(b)

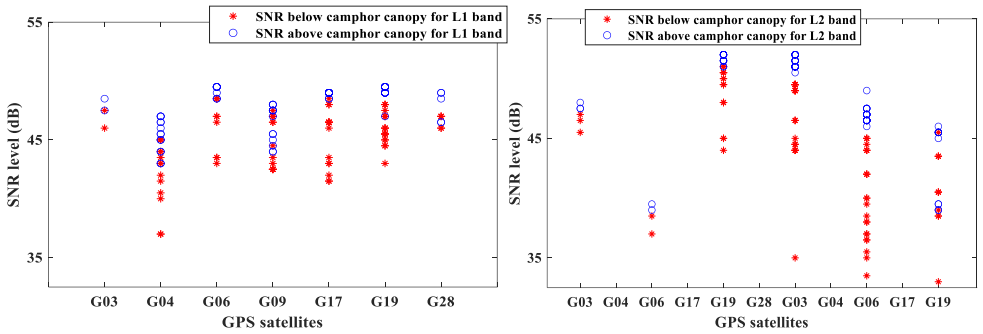
SNR below camphor canopy for L1 band
SNR above camphor canopy for L1 band
SNR level (dB)
55
45
35
G03 G04 G06 G09 G17 G19 G28
GPS satellites
SNR below camphor canopy for L2 band
SNR above camphor canopy for L2 band
SNR level (dB)
55
45
35
G03 G04 G06 G17 G19 G28 G03 G04 G06 G17 G19
GPS satellites

(c)

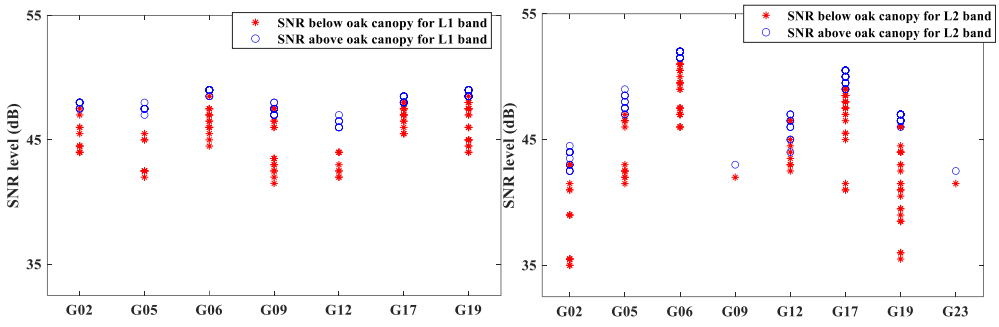
SNR below oak canopy for L1 band
SNR above oak canopy for L1 band
SNR level (dB)
55
45
35
G02 G05 G06 G09 G12 G17 G19
SNR below oak canopy for L2 band
SNR above oak canopy for L2 band
SNR level (dB)
55
45
35
G02 G05 G06 G09 G12 G17 G19 G23

(d)

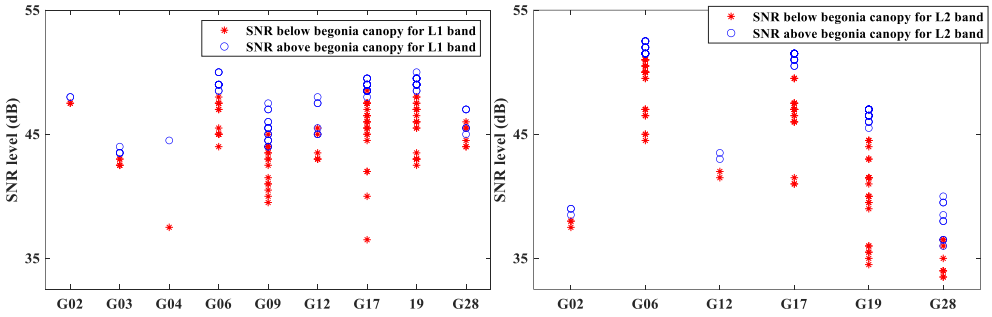
SNR below begonia canopy for L1 band
SNR above begonia canopy for L1 band
SNR level (dB)
55
45
35
G02 G03 G04 G06 G09 G12 G17 19 G28
SNR below begonia canopy for L2 band
SNR above begonia canopy for L2 band
SNR level (dB)
55
45
35
G02 G06 G12 G17 G19 G28

(e)

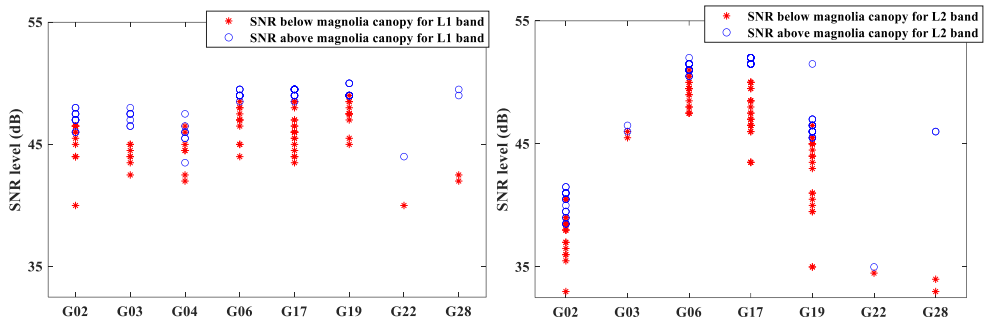

(f)

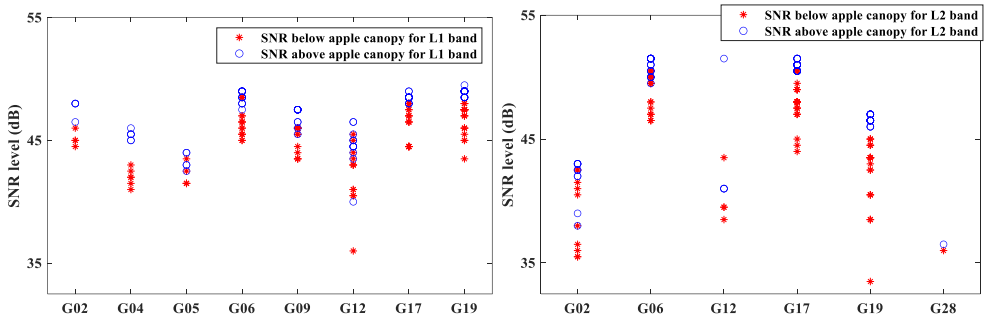

(g)

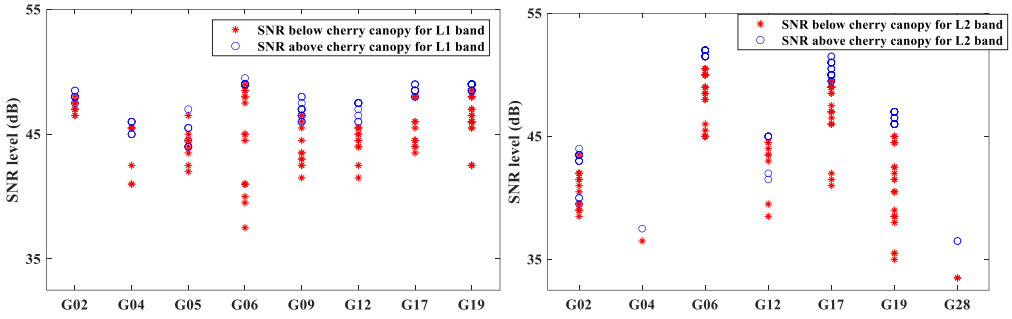

(h)

Figure 12. Received GPS signal levels from above- and below-canopy at the L1 and L2 bands for (a) osmanthus tree, (b) camphor tree, (c) purple-leaf plum tree, (d) oak tree, (e) begonia tree, (f) magnolia tree, (g) apple tree, and (h) cherry tree during the experiments.

In Figure 13, the statistical information of received signals is summarized and visualized with a boxplot, which creates a box plot for the received GPS SNR levels. In each box, the central mark indicates the median, and the bottom and top edges of the box indicate the 25th and 75th

percentiles, respectively. The whiskers extend to the most extreme data points that are not considered outliers, and the outliers are plotted individually using the '+' symbol.

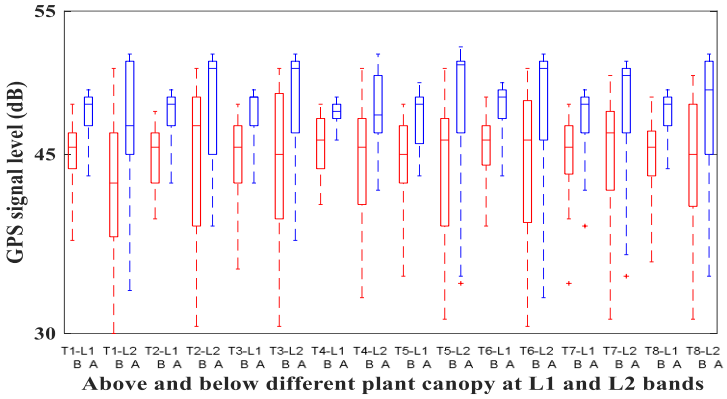

Figure 13. The statistical boxplot results of received GPS signals from above- and below-canopy at the L1 and L2 bands for the osmanthus tree, camphor tree, purple-leaf plum tree, oak tree, begonia tree, magnolia tree, apple tree, and cherry tree during the experiments.

The below-canopy signal levels are all lower than the signals received above the canopy, as indicated previously. The median value obtained below the canopy is also lower than that above the canopy. Moreover, the boxes of the L1 bands (below- and above-canopy) in Figure 13 are all shorter than the boxes of L2 bands observed from the eight tree types. This phenomenon indicated larger deviation was found with the L2 band compared to the L1 band, which may be due to the leaf size, or the incident angle may have an impact on the frequency, resulting in bigger variations. This phenomenon can be also seen in the following statistical table. Table 2 summarized and computed all data in the form of statistical metrics shown (Figure 13).

Table 2 The comparison of statistical SNR levels between the L1 and L2 bands.

SNR level	Below-canopy	Above-canopy

	Mean (dB)		SD (dB)		Mean (dB)		SD (dB)	
Tree name	L1	L2	L1	L2	L1	L2	L1	L2
Osmanthus tree	46.56	43.75	1.77	6.05	51.74	50.63	0.69	3.95
cherry plum tree	45.67	46.98	1.36	7.19	52.16	51.30	1.69	4.42
Camphor tree	46.00	46.89	2.98	6.31	52.67	51.48	1.63	3.60
Oak tree	47.16	47.05	1.79	4.83	52.17	51.39	0.41	2.19
Begonia tree	45.43	45.93	2.85	7.16	52.38	51.61	1.87	5.74
Magnolia tree	47.28	46.78	1.94	6.54	52.58	51.46	0.88	5.85
Apple tree	46.45	48.08	2.61	5.11	51.78	51.33	1.82	3.83
Cherry tree	46.16	46.63	2.68	5.24	52.60	51.62	0.81	4.27

Comparisons between the mean values and standard deviations (SDs) of the SNR in the L1 and L2 bands are summarized in Table 2. The mean value of the SNR below the canopy is lower than the values obtained above the canopy. Moreover, the attenuated SNR signal level varies with different types of trees. For both L1 and L2 band signals, the SD of the signal below the canopy is generally higher than the values above the canopy, which indicates that the GPS signals are quite sensitive to the canopy, which may largely be due to the results of the scattering phenomenon on the leaves.

Comparing the SNRs in the L1 and L2 bands, the SD obtained in the L2 band is higher than that in the L1 band, which agrees with the previous conclusion that a larger variation was observed in the L2 band. This phenomenon may be largely due to the scenario mentioned before. The leaf size, shape or the incident angle may have an impact on the frequency, resulting in bigger variations, and could be another subject of future work.

4.3. Model Fit as a Function of LAI to Signal Attenuations

The behavior and statistical results of the received above- and below-canopy signals are shown

above. A mathematical relationship between the collected LAIs and their corresponding attenuated SNR is shown with fitting models to reveal the effects of different LAIs on signal attenuations for both the L1 and L2 bands. Among all tracking satellites (Figure 10) during the experiment, the results of the most common satellites with high elevation angles (above 55°) during all measurements are selected and shown in the L1 and L2 bands. Figure 14 shows the relationship of different LAIs versus signal attenuations with four satellites G17, G19, G02, and G06 (in descending order of elevation angle) in both the L1 and L2 bands. The text box in each plot indicates the robust linear fit of the data (LAIs versus signal attenuations) and the Pearson correlation coefficient (R).

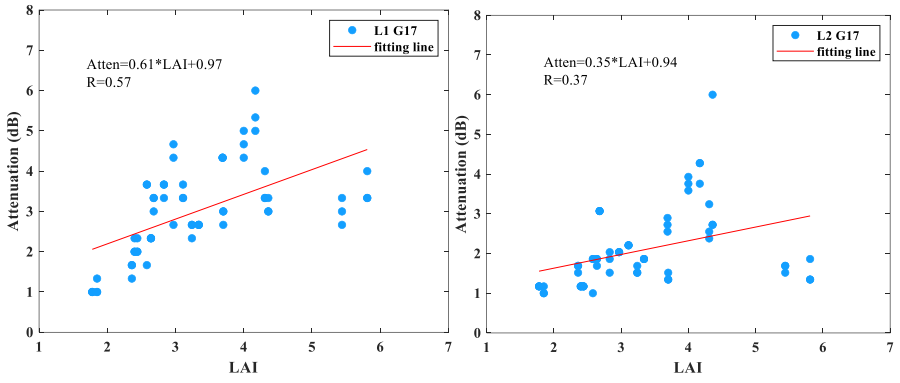

(a)

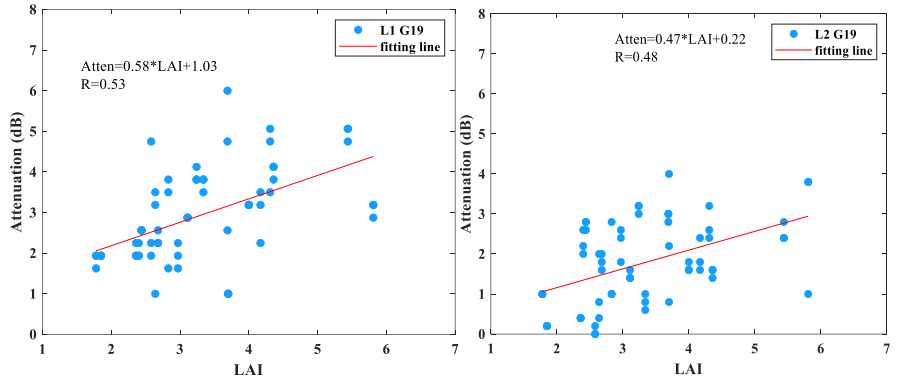

(b)

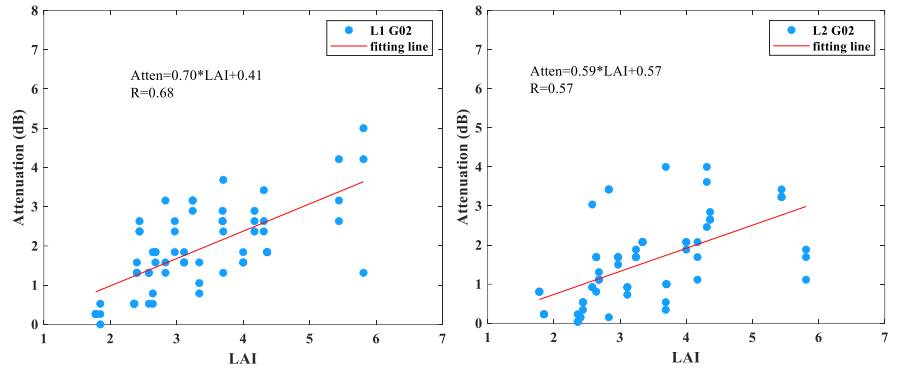

(c)

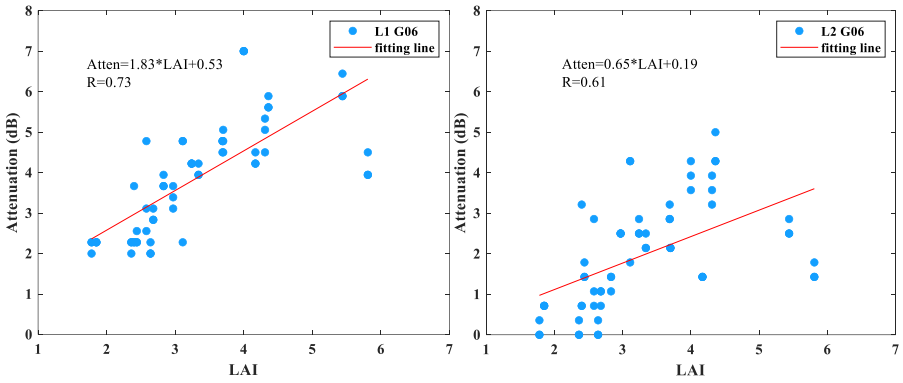

(d)

Figure 14. Scatter plot and robust fit of LAIs versus signal attenuation in the L1 and L2 bands for (a) GPS G17, (b) GPS G19, (c) GPS G02, and (d) GPS G06.

Figure 14 shows some sensitivity (Sv) of signal attenuations versus LAIs. LAI increases with increasing signal attenuation due to the influence of signal scattering and attenuation (increasing optical thickness). The lowest sensitivity occurs in the L2 band with GPS satellite G17, while the highest sensitivity of ~1.83 dB is observed in the case of the L1 band with GPS satellite G06. Moreover, the correlation coefficient R is considered acceptable. Notably, the sensitivity and R increase as the elevation angle decreases, which agrees with findings previously reported (Mehrez et al. 2018). This phenomenon can be seen clearly in Table 3 by comparing the results

for low-elevation satellites G02 and G06 to those for G17 or G19. However, the L1 band SV for G19 is slightly lower than that for G17, potentially due to some interference associated with the position of this satellite with respect to the receiving antenna.

Moreover, we noticed that the sensitivity to LAIs in the L1 band is higher than that in the L2 band, and the R values in the L2 band are lower than those in the L1 band for each GPS satellite. This phenomenon indicates that the GPS L1 signal is more sensitive and more correlated with LAI than L2, which could be explained by the fact that the L2 frequency is different from that of the L1 band, as well as the ranging code. The L2 band uses the frequency 1227.60 MHz, which has a longer wavelength than the L1, allowing the L2 signal to better travel through obstacles, such as cloud cover, trees, and buildings; hence, it is less sensitive and as related to LAI as the L1 band.

Table 3 The comparison of statistical parameters of the relationships in the L1 and L2 bands, Sv = the sensitivity of the GPS SNR attenuation to LAI.

	L1		L2	
	Sv ((dB/(m^2/m^2)))	abs(R)	Sv ((dB/(m^2/m^2)))	abs(R)
G17	0.61	0.57	0.35	0.37
G19	0.58	0.53	0.47	0.48
G02	0.70	0.68	0.59	0.57
G06	1.83	0.73	0.65	0.61

4.4. Fitting the Model as a Function of the LAI to Signal Attenuations over Different Tree Types

To further analyze this effect, the whole dataset was grouped based on the eight tree types. These trees have different profiles, which are shown in order of leaf size from small to large, corresponding to the photo from left to right in Figure 7. In this case, Figure 15 shows the robust fitting results over different types of trees. The corresponding statistical parameters for each tree are also presented (Table 4). Signal attenuations increase with increasing LAI. The sensitivity of

L1-band signal attenuations is 0.52 dB/(m^2/m^2), and the R of 0.61 is higher than that of the L2-band signal for all types of trees, which was caused by the high penetration ability of L2 observed in the previous subsection.

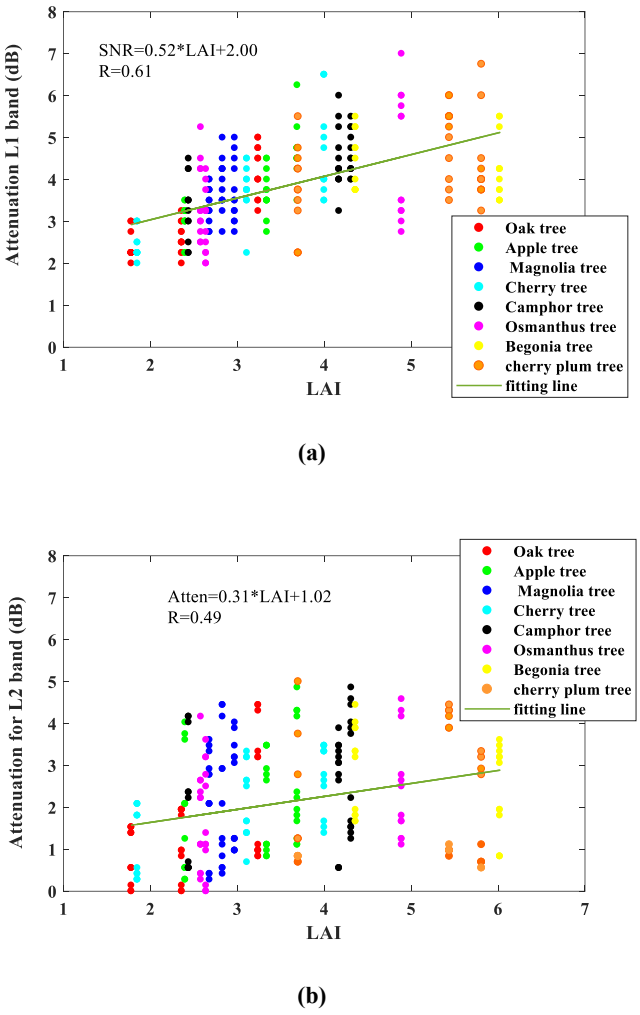

Figure 15. Scatter plot and robust fit of LAI versus signal attenuation in the L1 (a) and L2 (b) bands for different trees.

Table 4 shows the statistical parameters of the relationships between signal attenuations and LAIs corresponding to each tree type. The highest correlation parameter R = 0.85 and a very high sensitivity to LAIs ~ 1.30 dB/(m^2/m^2) in the L1 band demonstrate the large sensitivity of

signal attenuations to the LAIs of oak trees, which have the largest leaf size. Moreover, there is some sensitivity to the LAIs from the lowest 0.07 dB/(m^2/m^2) of camphor trees to the highest 1.30 dB/(m^2/m^2) of oak trees in the L1 band. This large difference can be attributed to the structure of the canopy and the leaf size, which could be observed from the tree photographs, as mentioned previously. The leaf sizes gradually decreased, and the branches became slenderer from the oak tree to the camphor tree. The signals more easily travel through the leaf surface or result in more diffuse scattering when the leaf size is smaller. The order of the photo (corresponding to the leaf size), which from small to large agree with the rules of sensitivity indicated by Table 4, suggests the structure of the canopy and leaf size also influences the signal acceptance, making these field experiments more significant. It is noted that the camphor tree has a unique feature that sets it apart from other well-known trees, which is its abundance of volatile essential oils. Camphor tree leaves are relatively smooth, shiny, and waxy, which may be the reason why their SV is not as significant compared to other trees.

Table 4 Comparison of statistical fitting behaviors in the L1 and L2 bands.

Tree type/SNR	L1		L2	
	Sv ((dB/ (m^2/m^2)))	abs(R)	Sv ((dB/ (m^2/m^2)))	abs(R)
Camphor tree	0.07	0.09	0.33	0.25
Purple-leaf plum tree	0.45	0.38	0.33	0.29
Begonia tree	0.59	0.51	0.34	0.29
Osmanthus tree	0.70	0.67	0.48	0.29
Magnolia	0.96	0.78	0.35	0.43
Cherry tree	1.07	0.78	0.74	0.63
Apple tree	1.16	0.74	0.78	0.64
Oak tree	1.30	0.85	1.06	0.52

5. Conclusions

In this study, a qualitative analysis of LAI and received GPS L-band signals is performed to investigate and obtain the impact of vegetation on GNSS signals based on the GNSS-R system. A GNSS receiver was employed to receive the above- and below-canopy signals. A powerful instrument, LAI-2200C, was adopted to evaluate the LAI for different types of trees. The scatter plots in the statistical results are also obtained. Then, the sensitivity of the received scattered power, including the received above-canopy SNR level, below-canopy SNR level, and the signal attenuations to LAIs, are analyzed in both the L1 and L2 bands for different types of trees and for a wide range of LAI values.

The below-canopy SNR is lower than the above-canopy SNR for each sampling unit. The received mean and median values of the below-canopy SNR are lower than those of the above-canopy SNR, and the SD value of the below-canopy SNR is higher than that of the above-canopy SNR. These expected results suggest that LAI plays a dominant role in the GNSS-R received, which may largely be due to the results of the scattering phenomenon on the leaves. Moreover, LAI and signal attenuation fitting models were built, indicating that the signal attenuation increases with increasing LAI. The mean SNR received in the L2 band is lower than that in the L1 band but with a larger standard deviation, which, in view of the rules observed for each satellite, indicates that the sensitivity values of the L1-band signal versus the LAI are higher than those of the L2-band signal. Moreover, the correlation coefficient between the L2-band signal and LAI is lower when compared to the L1-band signal for the same satellite. This result can be attributed to different factors but notably to the lower frequencies of L2 than L1, allowing the signal to better travel through obstacles.

The sensitivity and R are stronger when the elevation angle is smaller (Mehrez et al. 2018). The highest sensitivity to the LAI occurs at ~ 1.30 dB/ (m^2/m^2), and there is a high Pearson correlation (R = 0.85), indicating that the vegetation layer could largely attenuate the GPS signal. The sensitivity and correlation with the LAI increase with increasing leaf size (Camps et al. 2016). Despite the plant canopy attenuating the GNSS signals and reflectivity values, vegetation effects can be accounted for in GNSS-R SM retrievals using vegetation indices, such as the LAI, to compensate after the relationships between the LAI and attenuation are established.

This study provides certain insight for the further refinement of GNSS-R SM retrieval signal adoptions. It is important for GNSS-R SM retrieval to eliminate bias and improve accuracy, and the proposed approach could benefit other GNSS-R land applications or related surface-reflected signal studies. In future studies, field data that have been screened based on quantitative analysis could be used to compensate for the limitations of GNSS-R SM retrieval measurements and improve accuracy without using other auxiliary vegetation data.

Acknowledgments

This work was supported in part by the National Natural Science Foundation of China (under Grants 42001375, 42001362), by the Natural Science Foundation of Jiangsu Province (under Grant BK20180765), by the Nanjing Technology Innovation Foundation for Selected Overseas Scientists (under Grant RK032YZZ18003), by the NUPTSF (under Grant 219066), and by the Shanghai Leading Talent Project (Grant No. E056061) and Strategic Priority Research Program Project of the Chinese Academy of Sciences (Grant No. XDA23040100).

References

Alonso-Arroyo, A., A. Camps, A. Aguasca, G. F. Forte, A. Monerris, C. Rüdiger, J. P. Walker, H. Park, D. Pascual, and R. Onrubia. 2014. "Dual-Polarization GNSS-R Interference Pattern Technique for Soil Moisture Mapping." *IEEE J. Sel. Top. Appl. Earth Obs. Remote Sens.,* 7(5), 1533–1544.

Alonso-Arroyo, A., A. Camps, A. Aguasca, G. Forte, A. Monerris, C. Rüdiger, J. P. Walker, H. Park, D. Pascual, and R. Onrubia. 2014. "Improving the Accuracy of Soil Moisture Retrievals Using the Phase Difference of the Dual-Polarization GNSS-R Interference Patterns." *IEEE Geosci. Remote Sens. Lett.*, 11(12), 2090–2094.

Alonso-Arroyo, A., J. Querol, A. Camps, R. Onrubia, H. Park, and D. Pascual. 2016. "CAN WE MEASURE VEGETATION WATER CONTENT AND VEGETATION OPACITY AT L-BAND WITH A SINGLE GPS RECEIVER?" in *2016 IEEE Int. Geosci. Remote Sens*. Symp.

Arias, D., J. Calvo-Alvarado, and A. Dohrenbusch. 2007. "Calibration of LAI-2000 to estimate leaf area index (LAI) and assessment of its relationship with stand productivity in six native and introduced tree species in Costa Rica," *Forest Ecology and Management,* 247, 185–193.

Asner, G. P., J. Scurlock, and J. A. Hicke. 2003. "Global synthesis of leaf area index observations: implications for ecological and remote sensing studies." *Global Ecol Biogeogr*, 12(3), 191–205.

Ban, W., K. Yu and X. Zhang. 2017. "GEO-Satellite-Based Reflectometry for Soil Moisture Estimation: Signal Modeling and Algorithm Development. " *IEEE Transactions on Geoscience and Remote Sensing*, 56(3),1829-1838.

Behera, S. K., M. D. Behera, and R. Tuli. 2015. "An indirect method of estimating leaf area index in a tropical deciduous forest of India." *Ecol Indicat*, 58, 356–364.

Calabia, A., I. Molina, and S. Jin. 2020. "Soil Moisture Content from GNSS Reflectometry Using Dielectric Permittivity from Fresnel Reflection Coefficients." *Remote Sensing,* 12(1), 122.

Camps, A., H. Park, G. Portal, and L. Rossato. 2018. "Sensitivity of TDS-1 GNSS-R reflectivity to soil moisture: Global and regional differences and impact of different spatial scales." *Remote Sensing*, 10(11), 1856.

Camps, A., H. Park, M. Pablos, G. Foti, C. P. Gommenginger, P. W. Liu, and J. Judge. 2016. "Sensitivity of gnss-r spaceborne observations to soil moisture and vegetation." *IEEE Journal of Selected Topics in Applied Earth Observations & Remote Sensing*, 9(10), 4730-4742.

Camps, A., A. Adriano, H .Park, R. Onrubia, D. Pascual, and J. Querol. 2020. "L-band vegetation optical depth estimation using transmitted GNSS signals: Application to GNSS-reflectometry and positioning." *Remote Sensing*, 12(15), 2352.

Carreno-Luengo, H., G. Luzi, and M. Crosetto. 2019. "Sensitivity of cygnss bistatic reflectivity and smap microwave radiometry brightness temperature to geophysical parameters over land surfaces." *IEEE Journal of Selected Topics in Applied Earth Observations and Remote Sensing,* 12(1), 107-122.

Chen, J. M., and J. Cihlar. 1996. "Retrieving leaf area index of boreal conifer forests using landsat tm images. remote sensing of environment." *Remote Sensing of Environment*, 55(2), 153-162.

Chen, J. M., P. M. Rich, S. T Gower, J. M. Norman, and S. Plummer. 1997. "Leaf area index of boreal forests: theory, techniques, and measurements." *J Geophys Res*, 102(D24), 29429–29443.

Chen, J. M., and T. A. Black. 1992. "Defining leaf area index for non-flat leaves. Plant." *Cell Environ*, 15(4), 421–429.

Chen, Z., K. Yu, L. Jian, F. Wang, and Z. Yi. 2018. "Decreasing the error in the measurement of the ecosystem effective leaf area index of a pinus massoniana forest." *Journal of Forestry Research*, 30(4), 1459-1470.

Chew, C. C., and E. E. Small. 2020. "Description of the UCAR/CU Soil Moisture Product." *Remote Sens*. 12, 1558.

Chew, C. C., and E. E. Small. 2018. "Soil moisture sensing using spaceborne GNSS reflections: Comparison of CYGNSS reflectivity to SMAP soil moisture." *Geophys. Res. Lett.*, 45(9), 4049–4057.

Clarizia, M. P., N. Pierdicca, F. Costantini, and N. Floury. 2019. "Analysis of CyGNSS data for soil moisture retrieval." *IEEE Journal of Selected Topics in Applied Earth Observations and Remote Sensing,* 12(7), 2227-2235.

Clarizia, M. P., C. S. Ruf, P. Jales, and C. Gommenginger. 2014. "Spaceborne GNSS-R minimum variance wind speed estimator." *IEEE Trans. Geosci. Remote Sens.* 52, 6829–6843.

ComNav Technology Ltd.. Available online: https://www.81uav.cn/index.php?homepage=sinognss (accessed on 13th February 2023).

Egido, A., M. Caparrini, G. Ruffini, S. Paloscia, E. Santi, L. Guerriero, N. Pierdicca, and N. Floury. 2012. "Global navigation satellite systems reflectometry as a remote sensing tool for agriculture." *Remote Sens.*, 4(8), 2356–2372 .

Eroglu, O., M. Kurum, D. Boyd, and A. C. Gurbuz. 2019. "High spatio-temporal resolution CYGNSS soil moisture estimates using artificial neural networks." *Remote Sensing,* 11(19), 2272.

Fang, H., W. Li, S. Wei, and C. Jiang. 2014. "Seasonal variation of leaf area index (LAI) over paddy rice fields in NE China: Intercomparison of destructive sampling, LAI-2200, digital hemispherical photography (DHP), and AccuPAR methods." *Agricultural and Forest Meteorology*, 198, 126-141.

Ferrazzoli, P., L. Guerriero, and D. Solimini. 2000. "Simulating bistatic scatter from surfaces covered with vegetation." *J. of Electromagn. Waves and Application*, 14(2), 233-248.

Ferrazzoli, P., L. Guerriero, N. Pierdicca, and R. Rahmoune. 2011. "Forest biomass monitoring with GNSS-R: theoretical simulations." *Adv. in Space Res.* 47(10), 1823-1832.

Foti, G., C. Gommenginger, P. Jales, M. Unwin, and J. Rosello. 2015. "Spaceborne GNSS reflectometry for ocean winds: First results from the UK TechDemoSat-1 mission." *Geophysical Research Letters*, 42(13), 5435-5441.

GCOS G. 2011. "Systematic Observation Requirements for Satellite-Based Products for Climate, 2011 Update, Supplemental Details to the Satellite-Based Component of the Implementation Plan for the

Global Observing System for Climate in Support of the UNFCCC (2010 Update)." In Tech. rep. World Meteorological Organisation (WMO) 7 bis, avenue de la Paix, CH-1211 Geneva 2, Switzerland.

Gholz, H. L. 1982. "Environmental limits on aboveground net primary production, leaf area, and biomass in vegetation zones of the Pacific Northwest." *Ecology*, 63, 469–481.

Holland, P. W., and R. E. Welsch. 1997. "Robust regression using iteratively reweighted least-squares." *Commun. Stat. Theory Methods*, 6, 813–827.

Jia, Y., P. Savi, D. Canone, and R. Notarpietro. 2016. "Estimation of Surface Characteristics Using GNSS LH-Reflected Signals: Land Versus Water." *IEEE Journal of Selected Topics in Applied Earth Observations and Remote Sensing,* 9(10), 4752-4758.

Jia, Y., S. Jin, H. Chen, Q. Yan, P. Savi, Y. Jin, and Y. Yuan. 2021. "Temporal-spatial soil moisture estimation from CYGNSS using machine learning regression with a pre-classification approach." *IEEE J. Sel. Top. Appl. Earth Obs. Remote Sens.* doi:10.1109/JSTARS.2021.3076470

Jin, S., X. Qian, and H. Kutoglu. 2016. "Snow depth variations estimated from GPS-reflectometry: A case study in Alaska from L2P SNR data." *Remote Sens.*, 8(1), 63.

Jin, S., G. P. Feng, and S. Gleason. 2011. "Remote sensing using GNSS signals: Current status and future directions." *Advances in Space Research,* 47(10), 1645-1653.

Larson, K. M., J. J. Braun, E. E. Small, V. U. Zavorotny, E. D. Gutmann, and A. L. Bilich. 2010. "GPS multipath and its relation to near- surface soil moisture content." *IEEE J. Sel. Top. Appl. Earth Obs. Remote Sens*., 3(1), 91–99.

Law, B. E., T. S. Van, A. Cescatti, and D. D. Baldocchi. 2001. "Estimation of leaf area index in open-canopy ponderosa pine forests at different successional stages and management regimes in Oregon." *Agricultural and Forest Meteorology*, 108, 1–14.

Li, W., E. Cardellach, F. Fabra, A. Rius, S. Ribó, and M. Martín-Neira, 2017. "First spaceborne phase altimetry over sea ice using TechDemoSat-1 GNSS-R signals." *Geophysical Research Letters,* 44(16), 8369-8376.

Li, X., K. Zheng, L. Xin, G. Liu, M. Ge, W. Jens, and H. Schuh. 2019. "Real-time capturing of seismic waveforms using high-rate BDS, GPS and GLONASS observations: the 2017 Mw 6.5 Jiuzhaigou earthquake in China." *GPS Solutions*, 23(1), 17.

Li, Z. W., X. P. Xin, T. Huan, Y. Fan, B. R. Chen, and B. H. Zhang. 2017. "Estimating grassland LAI using the Random Forests approach and Landsat imagery in the meadow steppe of Hulunber, China." *Journal of integrative agriculture*, 16(2), 286-297.

Li-Cor. 1992. "LAI-2000 plant canopy analyser operating manual." Li- Cor Inc., Lincoln.

Lu, C., G. Feng, Y. Zheng, K. Zhang, H. Tan, G. Dick, and J. Wickert. 2017. "Real-Time Retrieval of Precipitable Water Vapor From Galileo Observations by Using the MGEX Network." IEEE Transactions on Geoscience and Remote Sensing, 58(7), 4743-4753.

Lowe, S. T., P. Kroger, G. Franklin, J. L. LaBrecque, J. Lerma, M. Lough, M. R. Marcin, R. J. Muellerschoen, D. Spitzmesser, and L.E. Young. 2002. "A delay/Doppler-mapping receiver system for GPS-reflection remote sensing." *IEEE Trans. Geosci. Remote Sensing,* 40(5), 1150-1163.

Masters, D., A. Penina, and S. Katzberg. 2004. "Initial results of land-reflected GPS bistatic radar measurements in SMEX02." *Remote Sens. Environ.*, 92 (4), 507–520.

Mehrez, Z., M. Erwan, B. Nicolas, F. Baup, D. Sylvia, F. Pascal, G. Dominique, H. Mireille, and W. Jean-Pierre. 2018. "Potential Applications of GNSS-R Observations over Agricultural Areas: Results from the GLORI Airborne Campaign." *Remote Sensing*, 10(8), 1245.

Mehrez. Z., M. Erwan, F. Pascal, and Z. Walid. 2017. "Low-cost GPS receivers for the monitoring of sunflower cover dynamics." *Journal of Sensors*.

Nasser. N., and S. Jin. 2013. "Physical Reflectivity and Polarization Characteristics for Snow and Ice-Covered Surfaces Interacting with GPS Signals." *Remote Sensing*, 5(8), 4006-4030.

Njoku. E. G., and D. Entekhabi. 1996. "Passive microwave remote sensing of soil moisture." *Journal of hydrology*, 184(1-2), 101-129.

Rodriguez-Alvarez, N., B. Holt, S. Jaruwatanadilok, E. Podest, and K.C. Cavanaugh. 2019. "An Arctic sea ice multi-step classification based on GNSS-R data from the TDS-1 mission." *Remote Sens. Environ.* 230, 111202.

Rodriguez-Alvarez, N., X. Bosch-Lluis, A. Camps, I. Ramos-Perez, E. Valencia, H. Park, and M. Vall-llossera. 2012. "Vegetation Water Content Estimation Using GNSS Measurement." *IEEE Geosci. Remote Sens. Lett.*, 9 (2), 282–286.

Rodríguez-Fernández, N., A. Al-Bitar, A. Colliander, and T. Zhao. 2019. "Soil moisture remote sensing across scales." *Remote Sensing*, 11(2), 190-194.

Ruf, C. S., S. Gleason, and D. S. McKague. 2018. "Assessment of CYGNSS wind speed retrieval uncertainty." *IEEE Journal of Selected Topics in Applied Earth Observations and Remote Sensing*, 12(1), 87-97.

Senyurek, V., F. Lei, D. Boyd and A. C. Gurbuz. 2020. "Evaluations of a Machine Learning-Based CYGNSS Soil Moisture Estimates against SMAP Observations." *Remote Sensing,* 12(21), 3503.

Vincent, G., C. Antin, M. Laurans, J. Heurtebize, S. Durrieu, C. Lavalley, and J. Dauzat. 2017. "Mapping plant area index of tropical evergreen forest by airborne laser scanning. a cross-validation study using lai2200 optical sensor." *Remote Sensing of Environment,* 198, 254-266.

Waring, R. H., and S. W. Running. 2007. "Forest Ecosystems: Analysis at Multiple Scales." Elsevier Academic Press, Burlington, USA.

Watson, D. J. 1947. "Comparative physiological studies on the growth of field crops: I. Variation in net assimilation rate and leaf area between species and varieties, and within and between years." *Annals of botany*, 11(41), 41-76.

Welles, J. M., and S. Cohen. 1996. "Canopy structure measurement by gap fraction analysis using commercial instrument." *J Exp Bot*, 47(302), 1335–1342.

Welles, J. M., and J. M. Norman. 1991. "Instrument for indirect measurement of canopy architecture." *Agron. J.* 83(5), 818–825.

Wu, X. and S. Jin. 2014. "GNSS-Reflectometry: Forest canopies polarization scattering properties and modeling." *Adv. Space Res.* 54(5), 863-870.

Yan, Q. and W. Huang. 2020. “Sea ice thickness measurement using spaceborne GNSS-R: First results with TechDemoSat-1 data." *IEEE J. Sel. Top. Appl. Earth Obs. Remote Sens*., 13, 577–587.

Yan, Q., and W. Huang. 2019. "Sea Ice Remote Sensing Using GNSS-R: A Review." *Remote Sens*. 11, 2565.

Yan, Q., W. Huang, S. Jin, and Y. Jia. 2020. "Pan-tropical soil moisture mapping based on a three-layer model from CYGNSS GNSS-R data." *Remote Sensing of Environment,* 247, 111944.

Zavorotny, V. U., K. M. Larson, J. J. Braun, E. E. Small, E. D. Gutmann, and A. L. Bilich. 2009. "A physical model of GPS multipath caused by land reflections: Toward bare soil moisture retrievals." *IEEE J. Sel. Topics Appl. Earth Obs. Remote Sens.*, 3(1).

Zhang, Y., J. M. Chen, and J. R. Miller. 2005. "Determining digital hemispherical photograph exposure for leaf area index estimation." *Agric Forest Meteorol*, 133(1/4), 166–181.